

Detection of potential overbreak zones in tunnel blasting from MWD data

Original

Detection of potential overbreak zones in tunnel blasting from MWD data / Navarro, J.; Sanchidrián, J. A.; Segarra, P.; Castedo, R.; Costamagna, E.; López, L. M.. - In: TUNNELLING AND UNDERGROUND SPACE TECHNOLOGY. - ISSN 0886-7798. - STAMPA. - 82:(2018), pp. 504-516. [10.1016/j.tust.2018.08.060]

Availability:

This version is available at: 11583/2751355 since: 2019-09-11T16:23:10Z

Publisher:

Elsevier

Published

DOI:10.1016/j.tust.2018.08.060

Terms of use:

This article is made available under terms and conditions as specified in the corresponding bibliographic description in the repository

Publisher copyright

(Article begins on next page)



Detection of potential overbreak zones in tunnel blasting from MWD data

J. Navarro^{a,*}, J.A. Sanchidrián^a, P. Segarra^a, R. Castedo^a, E. Costamagna^b, L.M. López^a

^a Universidad Politécnica de Madrid – E.T.S.I. Minas y Energía, Spain

^b DIATI, Politecnico di Turin, Italy

ARTICLE INFO

Keywords:

Rock mass
Under-excavation
Over excavation
Measurement while drilling (MWD)
Rock blasting

ABSTRACT

The damage from blasting to the remaining rock mass is analyzed with the purpose of developing a drilling index from measure while drilling (MWD) parameters, able to predict high risk of potential over- and under-excavated zones produced by blasting in the contour of a tunnel. A new methodology based on the comparison of scanner profiles of the excavated sections with the position of the contour blastholes, has been developed to obtain the excavated mean distance (EMD) between the blasthole and the excavated profiles at each MWD record position, which may be considered as a damage measure. MWD parameters, that describe the in-situ rock mass properties before the blast, are thoroughly normalized to remove external influences that may hide the actual response of the rig to rock mass properties and lead to wrong interpretations. 54 blasts, which comprise around 1700 contour blastholes, have been compared with more than 4000 excavated sections. A non-linear multiple-variable power-form model has been developed to predict the excavated mean distance as function of the normalized penetration rate, hammer pressure, rotation speed, rotation pressure and water flow parameters, and the lookout distance. These parameters combine the rotational, hydraulic and percussive mechanisms of the drill, and the confinement of the explosive charge with depth. Sources of uncertainty, unavoidable in the harsh condition in which the data were measured, such as drilling deviations, the scaling and primary support prior to scanning the excavated section, possible variations (unrecorded) in the explosive linear density, etc., have been assumed to be of random nature.

1. Introduction

Rock excavation in mining and tunneling frequently use cautious blasting techniques. The primary objective of blasting is to fragment rock to allow loading and haulage, without creating extensive damage to the remaining rock mass. As Andersson (1994) defined: “*Cautious blasting is a blasting that does not cause damage to the rock outside of the intended damage distance*”.

For a cautious blast design, the damage on the perimeter of the excavation is mainly induced by contour and buffer blastholes and it is created by a drop of strength, caused by the opening or shearing of newly generated or existing fractures or cracks (Scoble et al., 1997; Ouchterlony et al., 2002; Costamagna et al., 2018). In tunneling, damage can be categorized as major, minor or no damage, when there is rock falling, chips detachment or no visual damage, respectively (Costamagna et al., 2018). Damage assessment is analyzed through four main indexes: (i) Rock Tunneling Quality Index (Q-value, Barton et al., 1974) as classification of the ground condition for underground excavations; (ii) Blast Damage Factor (Hoek et al., 2002; Hoek, 2012) that estimates the global rock mass strength and the rock mass modulus; (iii)

Blast Damage Index (Yu and Vongpaisal, 1996) that correlates the mechanics and the effects of wave propagation into the rock mass; and (iv) failure approach index (Xu et al., 2017) that quantifies the rock mass damage through numerical simulations for tunnel support design.

Overbreak on the contour perimeter, which is defined as the void created during the excavation in excess of an established perimeter or pay line (Mahtab et al., 1997), is usually correlated with the damage extension zone which measures the quality of the blast. Overbreak and underbreak are mainly influenced by the geotechnical condition of the rock mass (rock disturbances and rock strength) and blast design parameters such as the explosive type, the charge concentration, the blast timing, the drill pattern and the drilling deviations (Ibarra et al., 1996; Oggeri and Ova, 2004; Singh et al., 2003; Singh and Xavier, 2005; Hustrulid, 2010; Johnson, 2010). Blasting affects the rock mass structure because of shock wave propagation (vibrations), gas pressure and stress redistribution (Singh et al., 2003; Hu et al., 2014).

Guidelines on construction have established an overbreak magnitude of 0.15–0.2 m and 0.1–0.15 m in crown and sidewalls, respectively (Mandal and Singh, 2009; Cunningham and Goetzsche, 1990). The maximum overbreak distance allowed depends on each national

* Corresponding author.

E-mail address: juan.navarro.miguel@upm.es (J. Navarro).

legislation and special terms can be arranged between the two parts in the contract (Olsson, 2010; Costamagna et al., 2018). For example, Scandinavian countries present similar regulations for tunneling excavation requirements (Anläggnings-AMA in Sweden, InfraRYL in Finland and the Norwegian Public Roads Administration, NPRA, in Norway; Olsson, 2010; SN, 2004; NPRA, 2004). Consequences of a bad drilling can be short pulls of the rounds, increase of rock reinforcement due to extra overbreak in the rock mass, longer scaling and mucking time and bad control of grouting.

To analyze the extension of the overbreak, studies have been carried out by comparing the laser profile of the excavated perimeter with the designed tunnel profile. Kwon et al. (2009) investigated the characteristics of the excavation damage zone (EDZ) in a tunnel construction and carried out a sensitivity analysis of the predicted EDZ with several rock mass parameters obtained from laboratory and in situ tests. They determined that in situ stress ratio, Young's modulus and EDZ were the three main parameters in rock mass behavior after blasting. Mandal and Singh (2009) measured the overbreak, dividing the contour profile in three sections: left wall, right wall and crown. They found that the crown is more affected by overbreak, due to the stress conditions in this zone. Kim and Bruiland (2009, 2015) estimated a tunnel contour quality index (TCI) based on overbreak distances of cross-section scanners, contour roughness and longitudinal overbreak variation in each blasted round. Costamagna et al. (2018), used scanned tunnel profiles to assess the overbreak of the excavated void in relation to the intended theoretical section, and correlated this with the rock mass conditions of each round.

Rock excavation techniques are highly influenced by the geo-mechanical properties of the rock mass (Oggeri and Ova, 2004; Singh et al., 2003; Singh and Xavier, 2005; Mahdevari et al., 2013). A site investigation for a tunneling project generally includes a description of the rock condition and a rough estimation of the rock mass structural properties; however, during the operation, unexpected anomalies that may influence the results of the operation often occur. Such anomalies can be detected by Measure While Drilling (MWD) system on modern jumbos. This has been described by Schunnesson (1997) as a drill monitoring system which logs drilling data at predetermined length intervals providing information of the operational parameters involved in drilling. For rotary drilling, Teale (1965) and Liu and Yin (2001) introduced the concept of specific energy (SE) as the energy required to excavate a unit volume of rock. Scoble et al. (1989) studied the variations of monitored parameters to define different geological formations. Hatherly et al. (2015) compared the MWD data with the geological rock conditions, obtained by geophysical logs, and demonstrated that if rotary speed and weight on bit are kept constant, MWD measurements can determine rock properties. Leung and Scheduling (2015) have developed a coal-seam detection model called SEM (modulated specific energy).

In relation to studies developed for percussive and rotary-percussive drilling, Schunnesson (1996) used the logged parameters of percussive drilling to develop a method for estimating Rock Quality Designation (RQD, Deere and Miller, 1966) based not only on the penetration rate and torque parameters, but also on their variation, which shows a close correlation with the presence of large discontinuities, fractures or major faults. Schunnesson (1998) and Hjelle (2010) introduced a new methodology to normalize percussive and rotary-percussive drilling parameters, to remove external influences generated by the blasthole length and the drill rig performance. Peng et al. (2005) and Tang (2006) proposed a method for void/fracture detection and for prediction of the rock mass properties based on drilling for roof bolting. They found that the feed pressure is a good detector of anomalies or discontinuities in the rock and is a good estimator of the rock mass strength. In addition, Peng et al. (2005) designed a new methodology for normalizing MWD parameters based on determining the performance of the machine when drilling the air (i.e. for no-load condition, outside the rock mass). This assesses how much feed pressure or rotation pressure is required for

running the machine itself. From the correlation of MWD data with rock mass geo-mechanical measures, Schunnesson et al. (2011) suggested a model for the hydraulic properties of the rock mass, based on the monitored water flow and water pressure during rotary-percussive drilling. Schunnesson et al. (2012) explained a methodology to assess rock strength ranges based on a MWD hardness index provided by Atlas Copco software. For that, they used Schmidt hammer to correlate MWD values with empirical rock strength measurements. Naeimipour et al. (2014) developed a void detection algorithm based on MWD parameters. The algorithm was calibrated on full scale experimental tests in concrete blocks with various strengths. Kahraman et al. (2016) found a strong correlation of the penetration rate with the uniaxial compressive strength (UCS), the Brazilian tensile strength, the point load strength and the Schmidt hammer. Van Eldert et al. (2018) assessed the extent of the damage zone from MWD parameters and ground penetration radar measurements recorded along the tunnel wall.

Finally, Atlas Copco AB, Sandvik and Bever Control have developed their own software (Tunnel Manager MWD, iSURE and Bever Control, respectively), as a tool for planning, administration and evaluation of drilling. From the MWD files collected, the blastholes can be represented in 3D, and hardness and fracturing maps are provided. The theoretical background for this information is however confidential.

Although there are many studies focused on the overbreak control by blasting effect on the one hand and on geological and geo-mechanical interpretation of the rock mass by using MWD on the other, no relation between MWD parameters and overbreak (i.e., under or over excavation with respect to the theoretical tunnel contour line) from blasting exists. This paper aims at developing an engineering tool, based on MWD parameters, able to predict high-risk of overbreak potential zones generated on the perimeter of a tunnel face excavated by blasting. For that, scanner profiles of excavated sections have been compared with the contour blastholes position, to obtain the excavated mean distance (EMD) created by each hole. Given that blasting variables (mainly explosive charge and timing) are constant in contour blastholes (as from blast reports), the overbreak and underbreak are considered mainly influenced by the geotechnical condition of the rock mass. Since the MWD system can characterize the rock mass condition of the blastholes, these measures can be correlated with the excavated mean distance (EMD) calculated along the depth of each blasthole. The analysis will match high over-excavated zones with highly fractured or softer rock masses before the blast, and low excavated measures with competent rock.

2. Data overview

The study has been developed in the underground extension work of the municipal wastewater treatment plant in Bekkelaget (Oslo), Norway. The facility comprises five caverns, a main access gallery of about 850 m length and other sections. The construction was developed in competent rock mass, composed by gneiss with small tonalite and quartzite intrusions. The Rock Tunneling Quality Index (Q-value; Barton et al., 1974), obtained from visual inspection of the tunnel face, was used as classification of the ground condition. Fig. 1 plots the Q-value versus the chainage for the rounds analyzed in the study. They comprise 54 rounds located between chainages 294–518 and 560–772 of the main gallery (making up more than 400 m). Fig. 1 also shows the classification of the rock mass based on the Q-value index; rock mass condition generally qualified as good and fair.

Data from the rig have been used to locate the contour blastholes and to compare them with the excavated profiles. A three-boom jumbo XE3C, manufactured by Atlas Copco, equipped with percussive-rotary top hammer drill, using semi-automatic ABC (Advanced Boom Control) was used to drill the analyzed blasts. Data comprises production face drilling holes of short length (4–5.5 m), using single rod (5.5 m length and 38 mm diameter) and 46 mm bit. Eight MWD parameters were logged during the drilling operation with a sampling interval of 0.1 m.

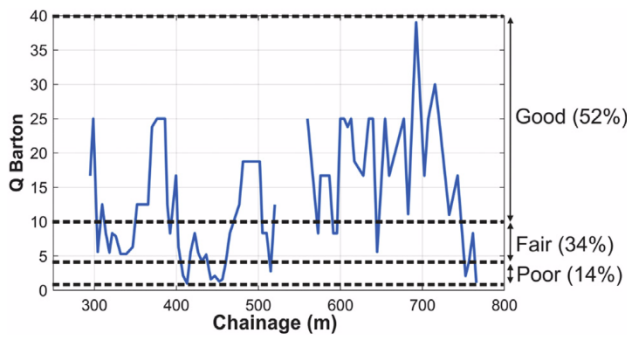


Fig. 1. Rock Tunneling Quality Index; Rock Tunneling Quality Index versus chainage and classification of the ground condition: poor ($1 < Q \leq 4$), fair ($4 < Q \leq 10$), good ($10 < Q \leq 40$).

These are described next as an extension of Peng et al. (2005), Beattie (2009), Hjelme (2010), Schunnesson et al. (2011), Schunnesson and Kristoffersson (2011) and Navarro et al. (2017) interpretations; the acronym and the units for each parameter are given in brackets.

- Feed Pressure (FP, bar): measure of the hydraulic pressure inside the cylinders. Feed pressure is required not only to keep the bit in contact with the bottom of the hole throughout the transmission of energy, but also to maintain a minimum force between bit and rock to maximize energy transfer to the rock.
- Hammer Pressure or Percussive Pressure (HP, bar): this is a measure of the impact pressure acting on the piston in the rock drill.
- Damp Pressure (DP, bar): it measures the pressure absorbed by the drill rig to prevent vibrations or undesired motion in the boom or drill rod.
- Rotation speed (RS, rpm): it is defined as the number of turns of the bit per minute.
- Penetration Rate (PR, dm/min): rate of penetration of the drill bit through the rock mass.
- Rotation Pressure (RP, bar): it is the torque pressure required to rotate the bit at a defined speed.
- Water Pressure (WP, bar): it is the pressure of the water used to flush the drill cuttings from the blasthole.
- Water Flow (WF, l/min): it is the rate of water inflow into the drill rod
- Hole Length (HL, m): depth at which each sample of the above parameters is logged.

The charging of the rounds was carried out with emulsion of different linear charge for different types of blasthole: cut, lifter, easer, buffer, contour. String loading method was used for the charging of the contour blastholes, with a design linear charge of 0.5 kg/m. This is assumed to be constant in the analysis. The actual charge of the holes may vary from the design value. However, such variations are assumed to be random so that, although they are a source of indetermination in the analysis, they will not bias the influence of the other parameters in the overbreak from blasting.

3. Analysis of the excavated area

3.1. Jumbo navigation

Navigation is necessary to locate the jumbo inside the tunnel before drilling a new round. For that, the jumbo rig uses three reference systems, sketched in Fig. 2: (i) an absolute coordinate system that references the position of the jumbo, in this case the EUREF 89 Norwegian Transverse Mercator (NTM) projection, (ii) a Tunnel Reference System (TRS) with one axis parallel to the tunnel axis and the other two in the plane of the tunnel face of the new round, and (iii) a Drilling Reference

System (DRS) defined by two vertical planes $X_d Y_d$, $Y_d Z_d$ and a horizontal $X_d Z_d$ plane. The angles of the TRS axes with the DRS ones are θ , ω and γ (see Fig. 2).

3.1.1. NTM coordinates system

The position of the jumbo inside the tunnel is first obtained, see Fig. 2 (i. NTM coordinate System). The jumbo has a laser scanner installed. In addition, target plates, with known coordinates, are located along the tunnel wall at every 5 m distance. The absolute coordinates of the jumbo are calculated by trilateration (i.e. distance measurement from the laser scanner to the target points). In this case study, X_{NTM} , Z_{NTM} coordinates are given in the NTM projection and Y_{NTM} is the height above sea level.

3.1.2. Tunnel Reference System (TRS)

The drill rig is aligned with the tunnel line (perpendicular line to the face of a new round that defines the orientation of the drilling) in order to follow the design of the construction. For that, two targets are mounted on one of the booms. The laser beam points to the free face in the direction of the tunnel axis and the boom is rotated until the laser beam passes through both targets (Fig. 2, ii. TRS). The boom is so aligned with the tunnel axis and the orientation and inclination of the boom are registered in three orthogonal vectors $(\vec{x}_t, \vec{y}_t, \vec{z}_t)$ to create a coordinate system parallel to the tunnel axis and the free face.

The laser scanner also measures the distance from the jumbo to the face of the new round and records the chainage at which it is located inside the tunnel. This chainage is taken as reference plane of the collaring depth position of the blastholes. Negative depth values are assigned to measurements behind this plane, and positive values, to measurements ahead of this plane.

3.1.3. Drilling Reference System (DRS)

The blasthole position measured by each boom is calculated in the Drilling Reference System defined by means of three spherical coordinates: blasthole length (l_b), azimuth or lookout direction (L_D) and inclination or lookout angle (L_I) (see Fig. 2):

$$X_F = l_b \cdot \sin(L_I) \cos(L_D) \tag{1}$$

$$Y_F = l_b \cdot \sin(L_I) \sin(L_D) \tag{2}$$

$$Z_F = l_b \cdot \cos(L_I) \tag{3}$$

The inclination angle varies between 0 and 90° both for holes drilled upwards or downwards so that the azimuth is between 0 and 180° for holes drilled upwards and between 0 and -180° for holes drilled downwards.

Blasthole positioning data logged by the ABC system uses sensors installed along the boom (outside the blasthole) to measure the azimuth and the inclination angles. The semi-automatic ABC total system installed in the drill rig authorizes the operator to move the boom and feeder manually to follow a predesigned drill plan (Navarro et al., 2018). Once the boom is placed in the required position and before the drilling starts, the measurements of the azimuth and inclination angles are logged in the DRS. These are considered constant as the boom remains still while drilling the blasthole. The end coordinates of the blasthole are calculated by adding, to their collaring coordinates, the result from Eqs. (1), (2) and (3). Since deviations beyond the collaring point cannot be measured by the MWD technology there is a possible error between the actual end position of the blastholes and the end position given by the MWD system. Drill deviations have not been monitored so they are a source of indetermination in our analysis that, as those mentioned in Section 2, is assumed to be of random nature.

3.1.4. Transformation system TRS-DRS

For Atlas Copco jumbos, the directional coordinate vectors of the TRS $(\vec{x}_t, \vec{y}_t, \vec{z}_t)$ and the NTM coordinates of the jumbo $(X_{NTM}, Y_{NTM},$

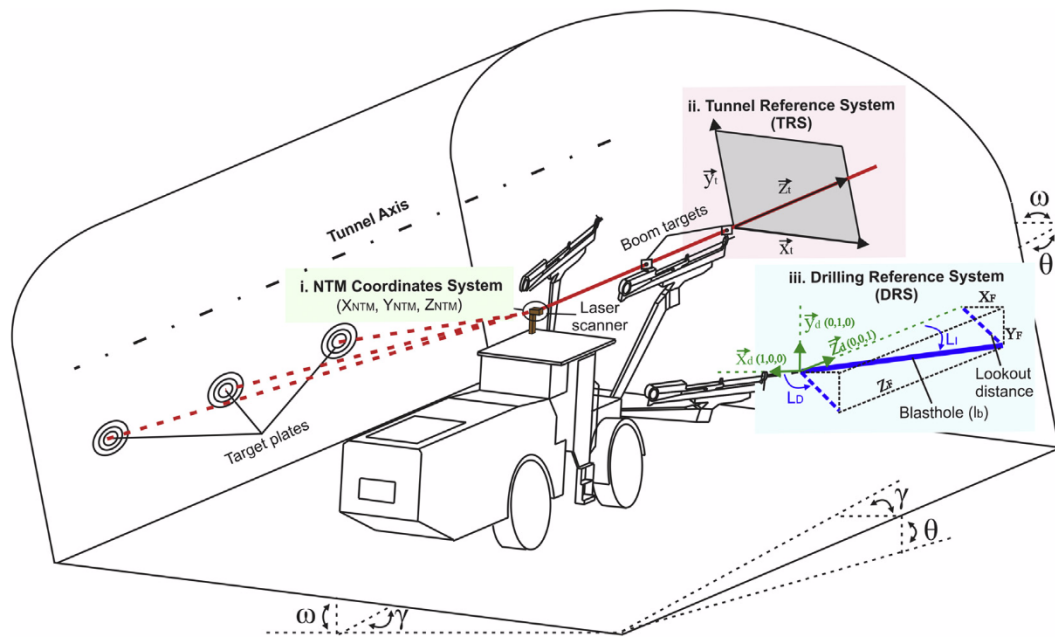


Fig. 2. Representation of the three reference systems involved in the jumbo navigation: i. NTM Coordinates System, ii. Tunnel Reference System, iii. Drilling Reference System.

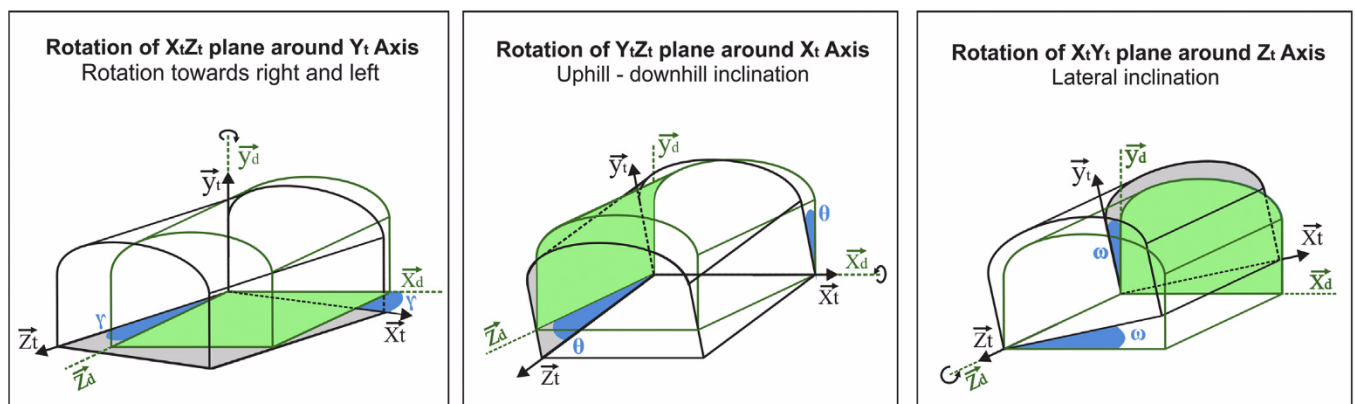


Fig. 3. Transformation from drilling reference system ($\vec{x}_d, \vec{y}_d, \vec{z}_d$) to tunnel reference system ($\vec{x}_t, \vec{y}_t, \vec{z}_t$). Left: Rotation towards right and left, or bearing angle, over \vec{y}_t ; center: uphill-downhill inclination, or elevation angle, rotation over \vec{x}_t ; right: lateral inclination, roll or bank angle, rotation over \vec{z}_t .

Z_{NTM}) are presented at the end of each MWD file. The three rotation angles to transform the DRS coordinates of a point in a borehole to the TRS can be seen in Fig. 2 and are further explained in Fig. 3.

This transformation is required below in order to know the exact position of the blasthole collars and their orientation. The location of the oriented blastholes in absolute coordinates ($X_{L,NTM}, Y_{L,NTM}, Z_{L,NTM}$) is obtained by adding the NTM coordinates of the jumbo ($X_{NTM}, Y_{NTM}, Z_{NTM}$) to the oriented coordinates of the blastholes (X_b, Y_b, Z_b) in the TRS system.

3.2. Superposition of excavated profiles and contour blastholes

A laser scanner system has been used to monitor the final profiles of the excavated void from each blast. The laser was located in the center of the excavation to be scanned and target spheres were installed along the wall of the main gallery in places with known coordinates. The software of the scanner identifies the position of the spheres in a post-analysis of the 3D cloud of points and trilaterates the location of the scanner by measuring distances from the laser to the spheres. Profiles of the excavated void in a direction perpendicular to the tunnel line are collected at steps of 0.2 m from the 3D cloud of points; each profile is

identified by its respective chainage. An interface AutoCAD-Matlab (AutoCad, 2017; Matlab, 2017) has been created to automatically compare the excavated profiles with the contour blastholes for each round. The profile formed by the contour holes (hereinafter named contour profile) is compared with the scanner profiles of the excavated sections in order to obtain the excavated mean distance between the blasthole and the scanner section at each depth for which MWD data are logged. This distance is considered as an indicator of the resulting damage (i.e. over-excavation).

For safety reasons, scanning of the excavated section is done after scaling and installation of primary supports. During scaling, non-stable rocks are removed from wall and roof to avoid rock falls and to ensure safe work conditions. Next, rock bolts and shotcrete are applied to reinforce the tunnel walls and to prevent stability problems. These operations obviously modify somewhat the perimeter excavated. Shotcrete was automatically applied to the tunnel surface and the thickness of the shotcrete layer was modified per round according to the geotechnical recognition of the tunnel wall and crown. The thickness of the shotcrete layer was known for every round and it was homogeneous over walls and crown, according to the operation reports. This thickness has been added to the scanner profiles in the AutoCad files to obtain the

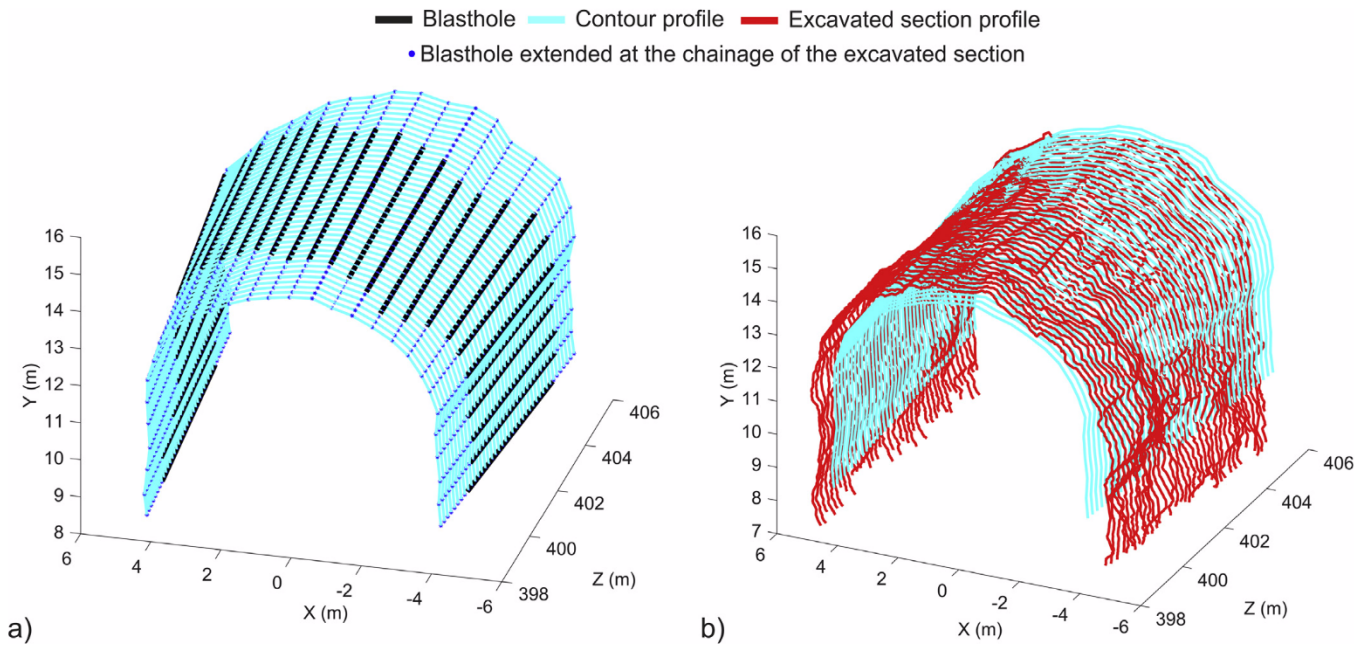


Fig. 4. Chainage 399. (a) Contour holes profiles and position of the blastholes; (b) Overlapping between the contour profiles and the excavated section profiles.

actual excavated contour from the blast. However, an unknown uncertainty still remains.

The comparison between excavated and contour profiles must take into account the lookout angle and lookout direction values for each blasthole, which make them to be outward oriented. Since no deviation data of the blasthole is available, it is assumed that the lookout increases linearly with depth. Eqs. (1) and (2) are used to calculate the theoretical position of the blasthole at each excavated profile depth in the local Drilling Reference System (DRS). Variables L_l and L_r are obtained from the MWD files and l_b is the length of the blasthole from the collaring position to the respective excavated profile depth (Z_{F_i} , see Fig. 2), obtained with Eq. (3).

Irregularities on the free face of a new round cause the collars of the blastholes not to be in the same plane, so they have different collar depths. In addition, some excavated profiles (mainly profiles at the beginning of the round) are not influenced by all contour holes of the current blast but for from the previous one. Each blasthole is extended from the foremost collaring hole to the depth of the deepest blasthole of each round to calculate the excavated area for all profiles included in a round. Fig. 4a represents the contour profiles (cyan lines), the position of the blastholes (black lines) and their extensions (tiny blue dots).

To carry out the analysis, both contour and excavated profiles must be overlaid. Excavated profiles from AutoCAD files are drawn in a vertical xy plane, where the Y coordinate is referred to the Y_{NTM} absolute coordinate and the hypothetical Z coordinate, i.e. depth of the xy plane, is indicated by the chainage at which it is located. The contour blastholes coordinates in the DRS must be rotated to the TRS. Since the rounds studied belong to the main gallery and they are excavated in a straight line, the xy and xz planes for both TRS and DRS coincide (angles γ and ω are 0); only plane y,z_i is rotated in case the tunnel axis is uphill (positive θ angle) or downhill (negative θ angle), see Fig. 3. The rotation of the DRS contour blastholes coordinates (X_d, Y_d, Z_d) to the TRS (X_r, Y_r, Z_r) is obtained by introducing the three angles ($\theta, \gamma = 0, \omega = 0$) in a 3D rotation matrix. The translation of the Y_t and Z_t coordinates is carried out by adding the Y_{NTM} and the chainage values of the round studied, respectively. Fig. 4b sketches the overlapping of both excavated (red lines) and contour holes (blue lines) profiles for a round.

3.3. Excavated mean distance from the blasthole

The overbreak created around the blasthole by blasting is caused, among other factors, by the combination of the explosive and the rock mass condition around the blasthole (Hustrulid, 2010; Johnson, 2010). Considering the contour blastholes position per round, an Excavated Mean Distance (EMD) has been defined (Fig. 5). It corresponds to the area between the midpoint of the spacing on both sides of the hole and the excavated profile, normalized by the distance between the midpoints of the spacing on both sides of the blasthole. When two adjacent holes are on the same side of the excavated profile, the EMD is calculated by (Fig. 5, EMD 1):

$$EMD = \frac{A_{T1}}{\frac{S_1}{2} + \frac{S_2}{2}} \tag{4}$$

where S_1 and S_2 are the spacing between the current blasthole and the

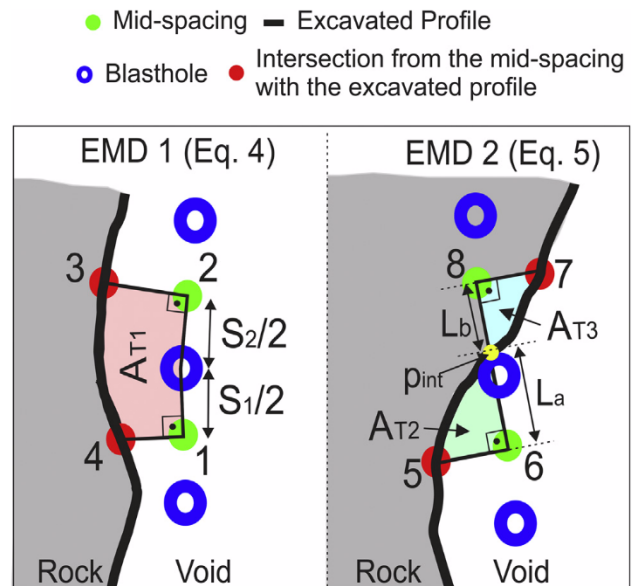


Fig. 5. Calculation of the Excavated Mean Distance.

adjacent ones (they are generally around 0.7 m); A_{T1} is the area excavated by each blasthole defined by points 1, 2, 3 and 4 in Fig. 5, EMD 1; it is positive when there is over-excavation and negative for under-excavation.

In case two consecutive blastholes are located one inside and the other outside of the excavated profile, corresponding to over and under-excavation (Fig. 5, EMD 2), the total excavated area is obtained by adding both areas with their respective sign:

$$EMD = \frac{A_{T2}}{L_a} + \frac{A_{T3}}{L_b} \tag{5}$$

where A_{T2} is the area defined by 5, 6 and p_{int} (Fig. 5, EMD 2); A_{T3} is the area defined by 7, 8 and p_{int} (Fig. 5, EMD 2); p_{int} is the intersection point between the excavated profile and the line joining two adjacent blastholes; L_a and L_b are the distances between p_{int} and the mid-spacing point between the current blasthole and the adjacent one.

The scanner profiles and the EMD values per blasthole are evaluated at 0.2 m intervals. The MWD sample interval is 0.1 m and the collaring chainage of each contour blasthole differs due to irregularities of the free face. Thus, the actual chainage of the MWD logs of each hole varies so that the position of the measurements recorded by the MWD system does not coincide with the depth of the calculated EMD values. A piecewise cubic Hermite interpolating polynomial (Fritsch and Carlson, 1980) is used to interpolate the EMD values at the specific depths of the MWD logs.

As an example, Fig. 6a shows the area of influence of each blasthole (AT1 or AT2 + AT3 in Fig. 5), calculated every 0.2 m for a round between the chainages 398 and 406 m; over- and under-excavated areas are plotted in different colors and the contour blastholes are marked in black. Fig. 6b represents the EMD values for one of the blastholes in graph a (that includes the backwards and forwards extensions, as explained above) versus chainage. It shows the EMD calculated (black dots), the cubic interpolation of the EMD calculated (red line), and the estimated EMD values corresponding to the MWD depths logged (blue dots).

4. MWD data processing

The response of MWD parameters is often affected by external influences different than the rock mass, such as the calibration of the

monitoring sensors, the hole length and/or the drill rig performance (Schunnesson, 1998). The control system of the jumbo, during the adjustment of the parameters while drilling, induces systematic variations in the MWD data. All together, they add uncertainty to the data that must be previously normalized in order to highlight changes in the parameters by the rock effect. This process comprises: (i) filtering out of unrealistic data, (ii) removing of the ramp-up section of the logs, (iii) correction of systematic variations in the MWD parameters such as the effect of hole length and feed pressure influence and (iv) normalization with the standard deviation to account for fluctuations in the signals. Fig. 7 shows a flow chart of the filtering and corrections applied to the raw MWD data, with the acronym used after each step.

4.1. Filtering of unrealistic values

Production data often includes unrealistic high and low performance values of the jumbo, which may lead to a wrong interpretation of the MWD data (Ghosh et al., 2015). A new filter of the data is developed before any further analysis. For that, the empirical probability distribution function of each MWD parameter is built from the complete data set values (54 blasts, comprising more than 6500 blastholes). The 95% confidence interval of MWD parameters defines the interval to retain data for the analysis. Fig. 8 shows the cumulative distribution functions (CDF) of the eight parameters, where the black dashed horizontal lines mark the 95% coverage and the vertical lines mark the corresponding limits of the parameters, given in Table 1.

4.2. Removing of ramp-up operation mode

The control system is normally based on three main operational modes (Schunnesson, 2017; Navarro et al., 2018): (i) collaring, (ii) ramp-up, both of which control the increase of the drilling pressure to minimize hole deviations, and (iii) normal drilling, which controls the performance of the parameters to optimize the operation and minimize damages to the drill system. As can be seen in Fig. 9, the feed pressure (FP) shows, initially, a sharp rise (ramp-up mode) until it reaches a pre-set threshold at which it stabilizes (normal drilling mode). Only values included in the normal drilling mode are considered for the analysis, as data in the ramp-up mode are not representative of changes in the rock mass conditions. Signals of the 8 parameters have been divided

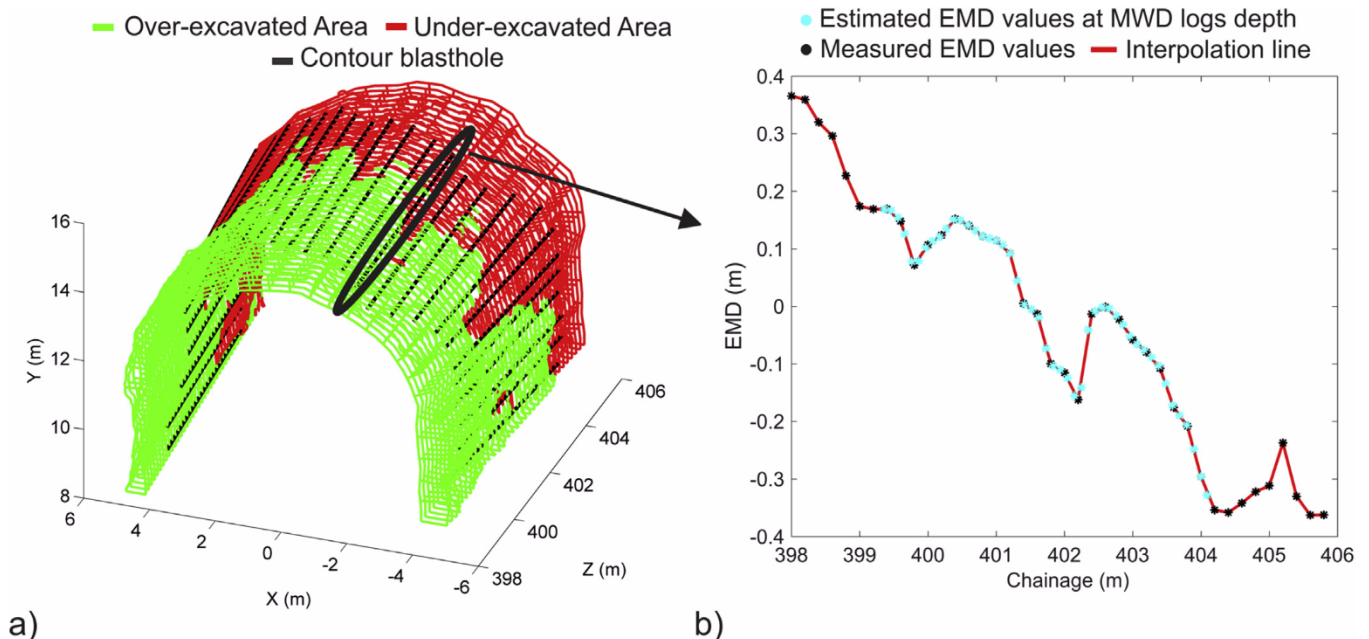


Fig. 6. (a) Area excavated along each blasthole; (b) EMD cubic interpolation and EMD value according to the MWD depth.

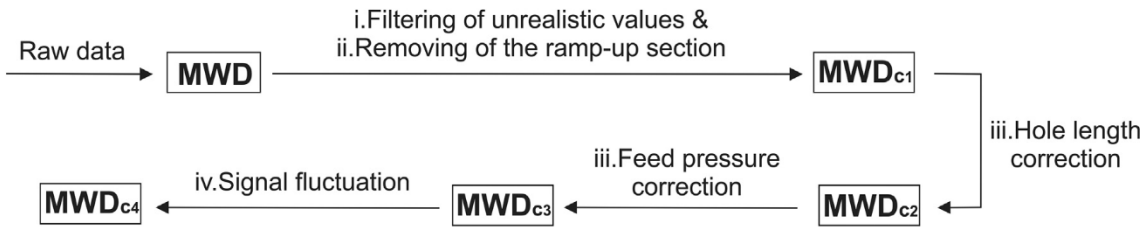


Fig. 7. MWD data processing flow chart.

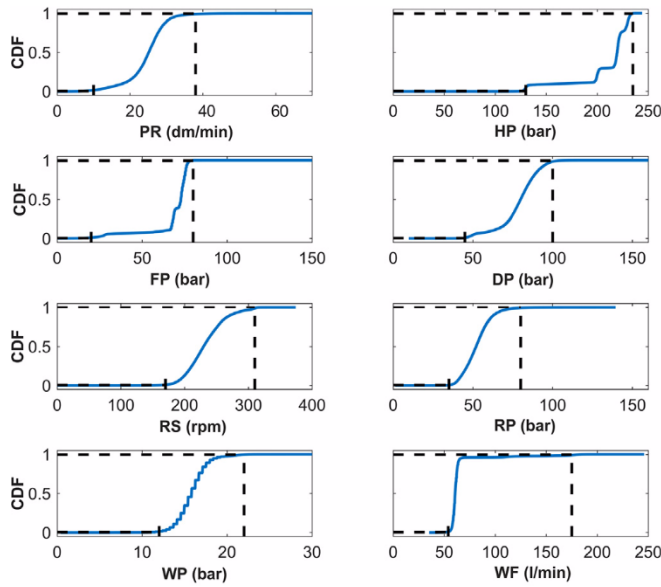


Fig. 8. Cumulative distribution function of the MWD parameters. Units and acronyms are given in Table 1.

Table 1
Range of reasonable values of the MWD parameters as from their 95% coverage.

Parameter	Acronym	Units	Range
Penetration rate	PR	dm/min	1–38
Hammer pressure	HP	bar	130–235
Feed pressure	FP	bar	20–80
Damp pressure	DP	bar	45–100
Rotation speed	RS	rpm	170–310
Rotation pressure	RP	bar	35–80
Water pressure	WP	bar	12–22
Water flow	WF	l/min	54–175

considering the point at which the feed pressure stabilizes. Values before this point comprise the ramp-up data set and forward values the normal drilling data set. The latter will be referred as MWD_{c1} .

4.3. Hole length and feed pressure corrections

Systematic variations generated by the drilling system and other parameters can be estimated and removed by averaging, for a large amount of data, the response of the parameters (Schunnesson, 1998; Hjelme, 2010). Schunnesson (1998), Hjelme (2010) and Ghosh (2017) described a significant hole length dependence in some parameters for percussive, rotary-percussive and Wassara water-hydraulic DTH drilling modes, respectively. This phenomenon is related to the increase of the frictional resistance between the drill rods and the blasthole walls, the reduction of the available pressure over the hammer, the reduction of the flushing efficiency with depth and the bit wear (Schunnesson, 1998). The average value of the eight MWD_{c1} parameters at every 0.1 m hole length has been calculated for the entire data from the 54 blasts

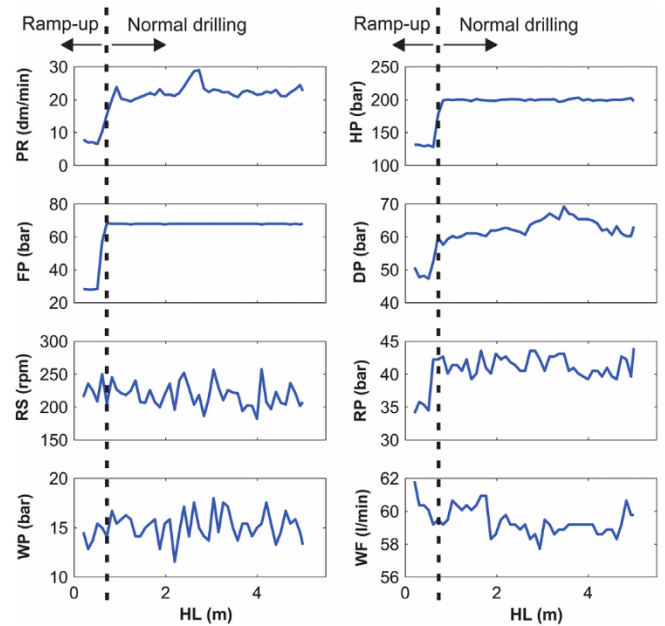


Fig. 9. Drilling operation modes in MWD signal from blasthole 71 at chainage 349. Units and acronyms meaning are given in Table 1; HL is hole length.

analyzed.

According to incidence reports, the sensors that monitor the position of boom 3 were out of calibration in most of the rounds, and the blastholes drilled by this boom had a lower lookout and lookout direction angles than recorded by the MWD files. This resulted in a systematic under-excavation in the contour profiles drilled by boom 3. The reports indicated a more intensive scaling on this side to meet the contour requirement. This results in a significant distortion of the excavated profile, hence in the over-excavated values calculated. Since the precise blasts for which boom 3 was out of calibration were not available, all data from boom 3 has been discarded for the analysis.

The correction of the hole length influence (to obtain a signal MWD_{c2} , see Fig. 7) is done by:

$$MWD_{c2}^i = [MWD_{c1}^i - MWD_{fit,HL}^i] + MWD_{fit,HL}^1; \quad \text{with } i = 1, 2, \dots, N \quad (6)$$

where i indicates each measurement in a hole log, N being the number of these. $MWD_{fit,HL}$ is a polynomial regression with hole length, of the average value at every 0.1 m hole length for the entire data of each MWD_{c1} parameter. $MWD_{fit,HL}^1$ is the intercept of the fit, i.e. the value at depth zero.

Fig. 10 shows the average MWD_{c1} signal (blue lines), the polynomial regression ($MWD_{fit,HL}$, green lines) and the hole length normalized average signal (MWD_{c2} , red lines), at every 0.1 m hole length for boom 1. The hole length normalization is not applied for the hammer pressure and for the water flow because there is no noticeable effect of depth in the average signal (see $Av.HP_{c1/c2}$ and $Av.WP_{c1/c2}$ in Fig. 10).

Previous work by the authors (Navarro et al., 2018) analyzed the relationship between MWD parameters to limit the number of the MWD

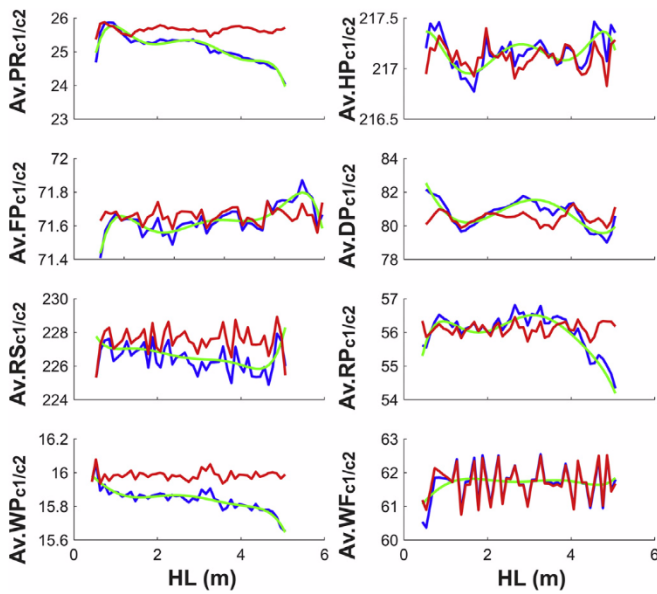


Fig. 10. Correction of hole length influence in MWD parameters (pass from MWD_{c1} to MWD_{c2} , see Fig. 7); blue lines: average signals, MWD_{c1} (obtained after filtering unrealistic values and removing ramp-up section, see Fig. 7); green lines: polynomial regression; red lines: average normalized signals, MWD_{c2} . Units and acronyms of the parameters in the ordinates are given in Table 1. (For interpretation of the references to color in this figure legend, the reader is referred to the web version of this article.)

variables, and to select the more significant ones that are required for a sound rock mass characterization. They did a cross-correlation analysis between the signals of the eight parameters in order to find leadership behaviors. The results pointed to the feed pressure as the lead parameter that drives the adjustment of the other variables to optimize the drilling. They showed that penetration rate, hammer pressure, damp pressure and rotation pressure are influenced by the feed pressure. According to this, the feed pressure generates systematic variations in these parameters that may hide the rock dependence on them. On the contrary, rotation speed, water flow and water pressure are little influenced by the feed pressure, thus being considered independent.

The same methodology followed for the hole length influence is now used to correct the feed pressure influence. The average value of the seven MWD_{c2} parameters (feed pressure is not included) is calculated at steps of 1 bar feed pressure value for the 54 blasts for boom 1. Similar to Eq. (6), the correction of the feed pressure influence (to obtain a signal MWD_{c3} , see Fig. 7) is done by:

$$MWD_{c3}^i = [MWD_{c2}^i - MWD_{fit,FP}^i] + MWD_{fit,FP}^1; \text{ with } i = 1, 2, \dots, N \quad (7)$$

where i indicates each measurement in a hole log, N being the number of these. $MWD_{fit,FP}^i$ is a polynomial regression with the feed pressure, of the average value at every 1 bar feed pressure for the entire data of each MWD_{c2} parameter. $MWD_{fit,FP}^1$ is the intercept of the fit, i.e. the value at the minimum feed pressure.

Fig. 11 shows the average MWD_{c2} signal (blue lines), the polynomial regression ($MWD_{fit,FP}$, green lines) and the feed pressure corrected average signal (MWD_{c3} , red lines), as function of the feed pressure. In line with Navarro et al. (2018), it can be seen that penetration rate (PR), hammer pressure (HP), damp pressure (DP) and rotation pressure (RP) parameters have a strong dependence from the feed pressure (FP). For the case of rotation speed (RS), water pressure (WP) and water flow (WF), the influence of feed pressure is considerably less, and these data are not normalized for the subsequent analysis; Fig. 11 shows no large differences between MWD_{c2} and the resulting MWD_{c3} signals for these parameters.

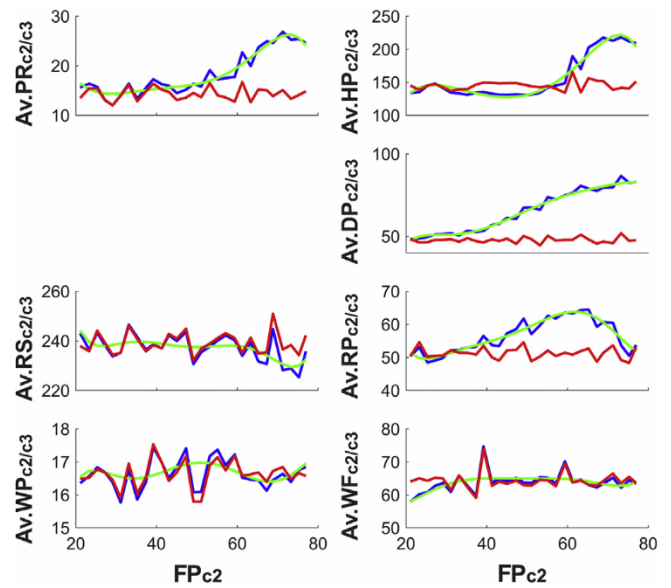


Fig. 11. Correction of the feed pressure influence in MWD parameters (MWD_{c2} conversion to MWD_{c3} , see Fig. 7); blue lines: average signals, MWD_{c2} (corrected for hole length influence, see Fig. 7); green lines: polynomial regression; red lines: average normalized signals, MWD_{c3} . Units and acronyms of the parameters are given in Table 1. (For interpretation of the references to color in this figure legend, the reader is referred to the web version of this article.)

4.4. Analysis of fluctuations in the MWD signals

Schunnesson (1996, 1997) claimed that when discontinuities in rock are drilled, penetration rate and rotation pressure show significant fluctuation, resulting in a noisy signal. Following this reasoning, parameters involved in the rotational mechanism of the jumbo (rotation pressure and rotation speed) and the penetration rate have been processed. The procedure is carried out for the signal of each hole individually, where the MWD_{c3} values in a hole are divided by the standard deviation of the entire signal of that hole. The resulting signals for these three parameters are MWD_{c4} .

$$MWD_{c4}^i = \frac{MWD_{c3}^i}{std(MWD_{c3})}; \text{ with } i = 1, 2, \dots, N \quad (8)$$

where i indicates each measurement in a hole log, N being the number of samples per signal.

5. Detection of potential overbreak zones

The processed penetration rate (PR_{c4}), hammer pressure (HP_{c3}) and rotation pressure (RP_{c4}) result in rock dependent parameters. The normalized rotation speed (RS_{c4}) and water flow (WF_{c3}) are independent parameters sensitive to rock variations (Navarro et al., 2018). The response of these normalized parameters can detect variations in the rock and for equal blasting conditions they may explain variations in EMD data. The feed pressure is not considered as it has been used during the normalization.

The lookout distance (i.e. distance from the collaring to the position of the hole in the XY plane at each depth, see Fig. 2) is also considered for the analysis as it may reflect the confinement effect by depth. Fig. 12a shows, as an example, variations of EMD with the hole length and lookout distance for the holes of the blast located at the chainage 500. As can be seen, there is a negative influence of the lookout in the EMD which means that the excavated area in relation with the blasthole position decreases with the lookout distance; this EMD relation with lookout distance is the same as with hole length since the lookout distance increases with depth. An increase of confinement with lookout

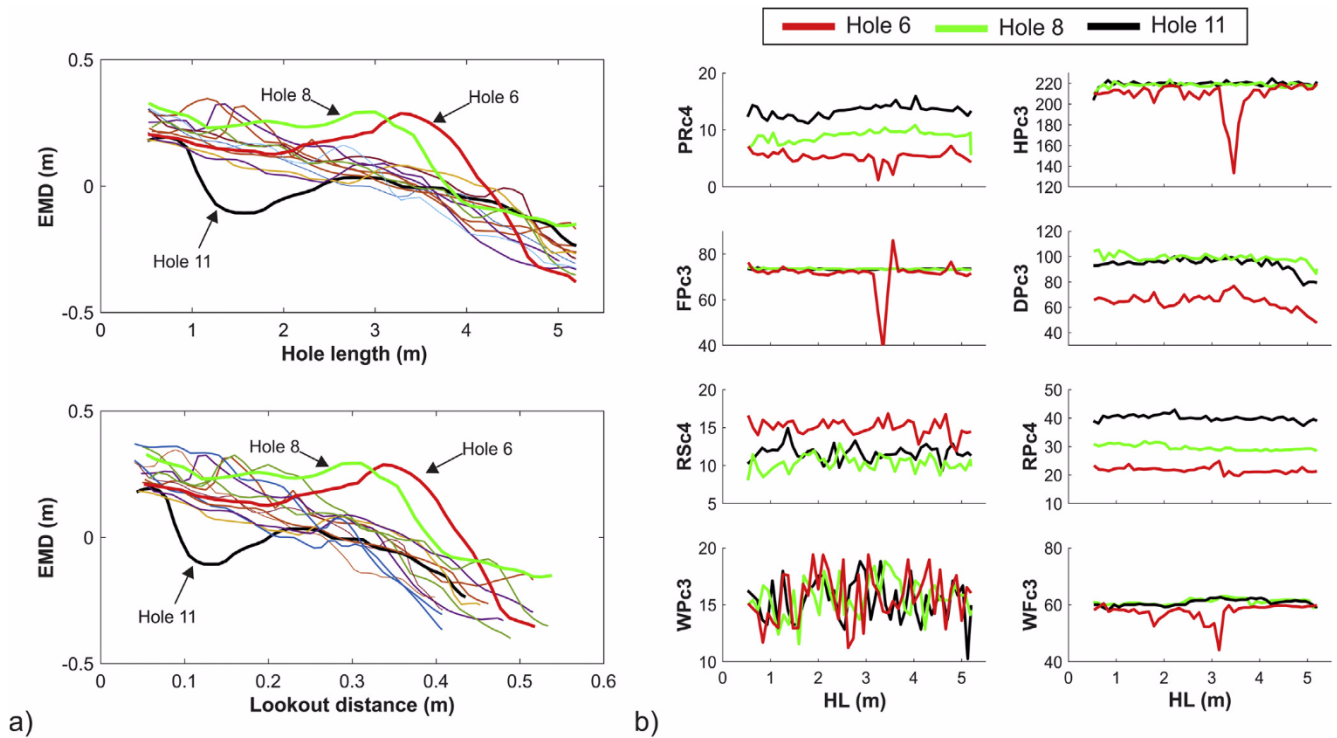


Fig. 12. Preselection of the data for blastholes of boom1 at the chainage 591; (a) EMD vs. hole length and lookout distance; (b) MWD signals for blastholes 6, 7 and 11. See Table 1 for the acronyms of MWD parameters; subscripts c₃ and c₄ refer to the corrections shown in Fig. 7.

distance and depth is associated with an increase of the difficulty in breaking the rock, resulting then in a decrease of the over-excavated area, hence the EMD, which may be even negative (under-excavation). Therefore, the larger the lookout distance and the deeper the drilling, the more under-excavation is created in relation with the position of the contour blastholes. In some cases (data for holes 6, 8 and 11, Fig. 12a), the general trend is not followed. Fig. 12b shows the respective MWD_{c3} and MWD_{c4} logging for holes 6, 8 and 11. One may think that local rock conditions may cause such results and that MWD parameters should show a peak or some kind of variation in the signal. This is effectively observed for hole 6, where MWD_{c3-c4} parameters show a significant peak or signal fluctuation at depth 3–4 m, in line with the over-excavation peak represented in graph a for this hole. However, no distinctive variation appears in the MWD_{c3-c4} records of holes 8 and 11. Hole 8 shows an over-excavated section at 2.5–3.5 m, whereas hole 11 indicates under-excavation at depth 1–2 m, though no significant changes can be observed in the MWD signal of these two holes at any depth. Other causes like drill deviations, malfunctioning of blasting, scaling, etc. may be behind such EMD outlier profiles, uncorrelated with the MWD logs; these outliers, that happen at most in one or two holes per blast (many blasts do not show any) are removed from the analysis.

Table 2 shows the statistics for the MWD_{c3} and MWD_{c4} parameters, the lookout distance, and the EMD values for boom 1.

A power function of the MWD parameters to predict the EMD is considered:

$$EMD = A_0 + PR_{c4}^{A1} \cdot HP_{c3}^{A2} \cdot RS_{c4}^{A3} \cdot RP_{c4}^{A4} \cdot WF_{c3}^{A5} \cdot L_{dist}^{A6} \quad (9)$$

where L_{dist} is the lookout distance.

Since EMD has positive and negative values, an additive constant A_0 has been included. The normalized damp pressure and water pressure have been removed since their contributions were found minimal. The non-linear regression model has been programmed with Matlab 2016b by a Levenberg-Marquardt non-linear ordinary least squares method (Matlab, 2016). The model coefficients are given in Table 3.

The determination coefficient of the fit R^2 is 0.74. Coefficient values

Table 2
Statistic of the MWD_{c3} and MWD_{c4} parameters for boom 1.

Parameter	Units	Mean	Std. ^a	Min.	Max.
Penetration rate _{c4}	m/min	13.01	9.40	0.04	57.10
Hammer pressure _{c3}	bar	211.81	15.04	63.00	230.0
Feed pressure _{c3}	bar	73.94	5.71	21.20	79.89
Damp pressure _{c3}	bar	65.31	12.76	48.23	86.63
Rotation speed _{c4}	rpm	34.73	30.91	0.18	98.58
Rotation pressure _{c4}	bar	26.55	12.99	0.09	128.05
Water flow _{c3}	l/min	81.99	28.20	53.70	145.56
Water pressure _{c3}	bar	16.43	4.87	13.57	21.84
Lookout	m	0.27	0.15	0.02	0.94
EMD	m	0.25 ^b	0.30	-0.63	1.09

^a Std. is standard deviation.

^b Mean absolute Value.

estimated for each parameter are significantly different from zero, i.e. their p-value is < 0.0001 for all cases, which means that the analysis is statistically significant. According to the value and sign of the coefficients, the MWD parameters affect EMD differently:

- The normalized penetration rate (PR_{c4}) and rotation pressure (RP_{c4}) show negative correlation (negative sign in A_1 and A_4) with EMD. According to Schunnesson (1996, 1997), high fluctuations in the PR and RP signals indicate soft/fractured rock. High fluctuations mean high standard deviation so that, according to Eq. (8), PR_{c4} and RP_{c4} show low values. This means that low PR_{c4} and RP_{c4} values indicate soft/fractured rock, prone to suffer over-excavation. The contrary is also true.
- The normalized hammer pressure (HP_{c3}) also shows a negative correlation with EMD (negative sign in A_2), which indicates that, when discontinuities or soft rock is drilled, the hammer of the boom needs a lower pressure to hit the rock. As explained by Peng et al. (2005) and Navarro et al. (2018), when open fissures or softer rock are found, the feed pressure shows a sharp drop to the level of drilling the air. This behavior is also noticed in the hammer

Table 3
Non-linear regression model coefficients.

	A_0	PR_{c4} A_1	HP_{c3} A_2	RS_{c4} A_3	RP_{c4} A_4	WF_{c3} A_5	L_{dist} A_6
Coefficient	-2.8432	-0.0341	-0.1188	0.0352	-0.0108	0.0834	-0.0600

pressure; in open fissures, there is no resistance for the hammer to hit the rock which results in a reduction of its pressure to avoid damage in the system. In this way, low hammer pressures values are related with over-excavated areas and vice versa.

- The normalized rotation speed (RS_{c4}) shows positive correlation with EMD (positive sign in A_3). Schunnesson (1998) claimed that at high feed pressure, the rotation pressure required for the rotation of the bit increases and sometimes a reduction in the rotation speed can be appreciated. The higher resistance to rotate may also translate into an increase in the signal fluctuation. According to Eq. (8), the higher the standard deviation of the RS parameter, the lower the RS_{c4} and the lower the excavated area is created, hence the positive sign of its exponent in Eq. (9). For the case of discontinuities, Hustrulid (1968) showed that at low feed pressure, the bit will not be in constant contact with the bottom of the hole, resulting in a free rotation of the bit that may show a lower fluctuation in the rotation speed. This way, the lower the standard deviation of the RS parameter, the higher the RS_{c4} and the greater the excavated area.
- The normalized water flow (WF_{c3}) has a positive correlation with EMD (positive sign in A_5). This can be explained by the fact that, when discontinuities or soft rock is drilled, the control system requires a higher water flow due to the higher amount of drill cuttings or the water leakage to the discontinuities.
- The lookout distance presents a negative correlation with EMD, which means, as discussed before, that the excavated area in relation with the blasthole position decreases with an increase of depth and lookout.

The results of the EMD predicted with the suggested model versus the EMD data are plotted in Fig. 13a. The linear regression obtained has a slope of one with a zero-constant term. Fig. 13a also shows the upper

and lower prediction band at a 95% confidence level. The residuals are normally distributed (see Fig. 13b).

Fig. 13c shows the distribution of the root mean square error (RMSE) for each of the 54 blasts. The median and the 25th and 75th percentiles of RMSE are 0.142 m, 0.102 m and 0.186 m, respectively. An illustration of the application of the model is shown in Fig. 14 for three blasts, representing the 75% (large error, Fig. 14a), 50% (expected error, Fig. 14b) and 25% (small error, Fig. 14c) of the RMSE values; they correspond to blasts located at the chainages 388, 500 and 591, respectively. In the three cases, the EMD predicted is compared with the EMD measured for blastholes of boom 1. Five different over-excavation ranges have been defined. For high RMSE values (Fig. 14a), visual differences between the predicted EMD and the EMD measured are apparent; these are considerably reduced when representing medium and low RMSE values (Fig. 14b and c). Fig. 14c shows a predicted EMD generally in line with the EMD measured though still some light differences exist. Considering the noise of the MWD data – unavoidable in the harsh conditions where such data are measured – and the additional uncertainty brought by drilling deviations, the scaling and primary support done before scanning the excavated section, sensors potentially out of calibration, possible variations in the explosive linear density, etc., the quality of the fit is outstanding.

6. Conclusions

The overbreak of the remaining rock mass in tunnel blasting has been analyzed in the light of MWD records, with the purpose of developing a prediction model of over- and under-excavation depths from blasting. Such predictive model may also be seen as a drill or rock index that could be used to identify zones of potentially high geotechnical risk (those for which the over-excavation prediction is high). By comparison

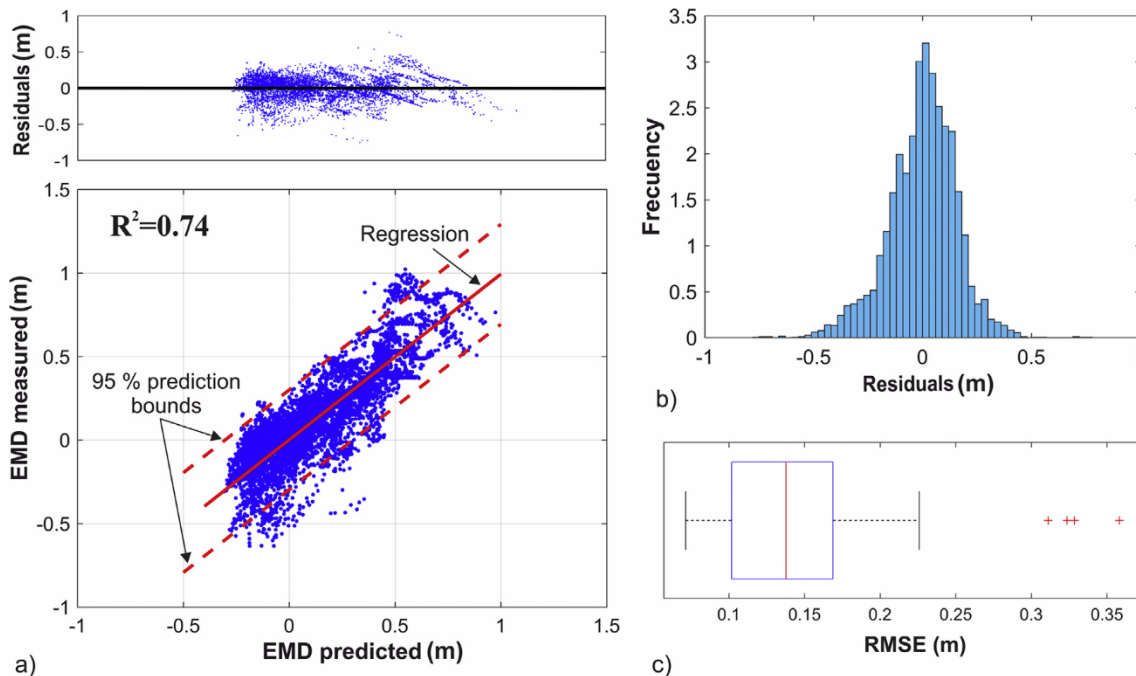


Fig. 13. Result of the EMD predicted model: (a) predicted versus measured EMD values (upper graph: residuals); (b) Box-plot of the RMSE values per blast.

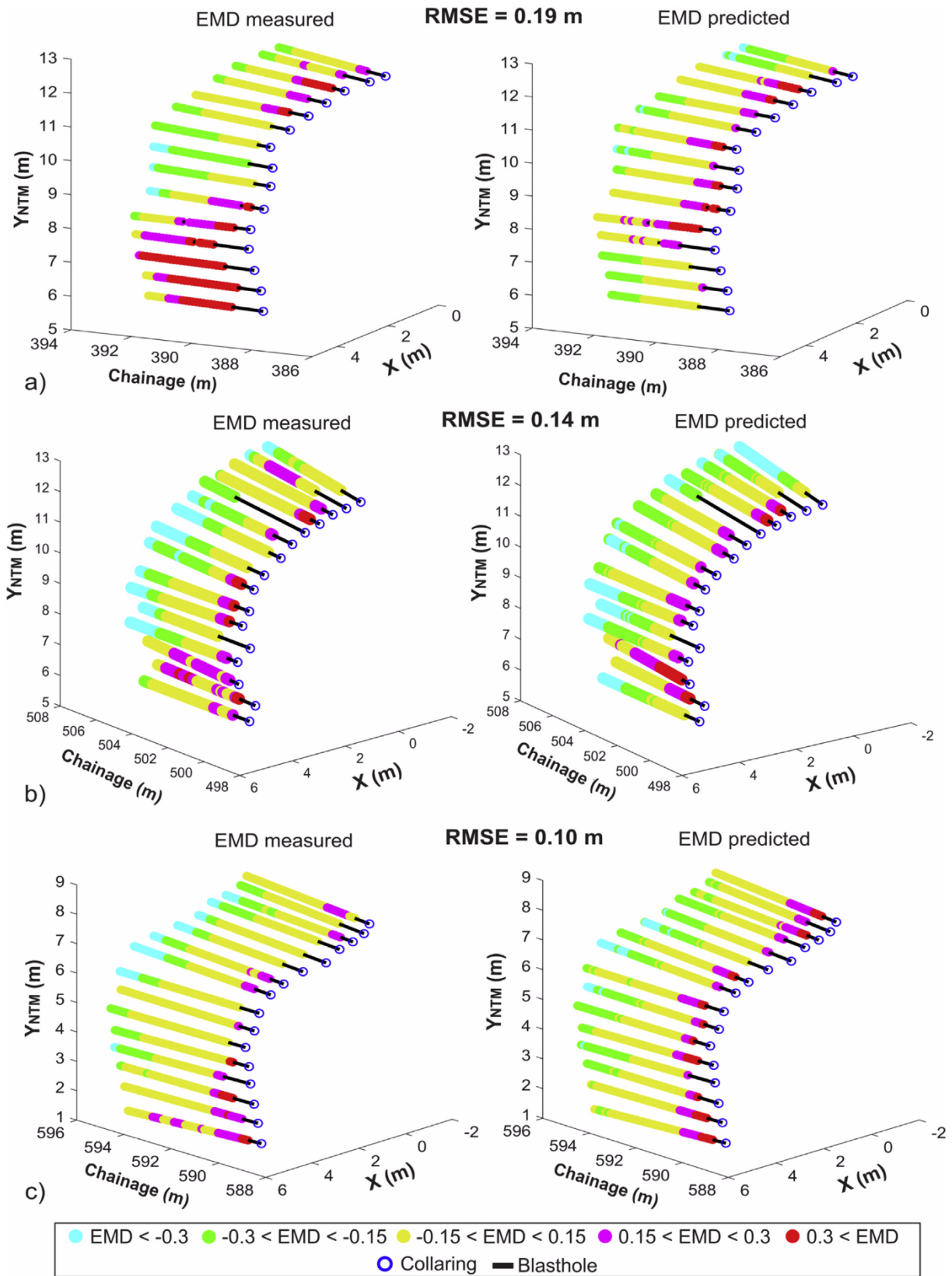


Fig. 14. Representation of the predicted EMD model (right graph) and the EMD measured (left graph) for blastholes of the boom 1: (a) blast in chainage 388, 75th percentile of the RMSE; (b) blast in chainage 500, median value of the RMSE; (c) blast in chainage 591, 25th percentile of the RMSE.

of scanner profiles of the excavated sections with the blasthole positions, a methodology has been developed to obtain an Excavated Mean Distance (EMD) between the blasthole and the excavated profile, which

may be considered a damage measure. Sources of uncertainty such as drilling deviations, the scaling and primary support done before scanning the excavated section, possible variations (unrecorded) in the

explosive linear density, etc., are assumed to be of random nature, unavoidable in the harsh condition in which such data are measured. Quantitative predictions for different conditions would require a recalibration of the model for the new site, following the methodology described here.

Given that blasting factors are constant (as from blast reports) the overbreak and underbreak are considered mainly influenced by the geotechnical condition of the rock mass. Such rock mass properties are assessed from MWD parameters that show the response of the jumbo to the rock before blasting. A thorough transformation of the MWD logs has been carried out to filter out systematic variations due to the nature of the drilling process and to highlight the dependence of the rock in the parameters. This transformation includes: (i) filtering out of unrealistic data, (ii) removal of the ramp-up section of the logs, (iii) normalization of systematic variations in the MWD parameters so that the influence of hole length and feed pressure are corrected and (iv) normalization with the standard deviation to account for fluctuations in the signals.

A non-linear power-form model has been developed that predicts the excavated mean distance as function of the normalized penetration rate, hammer pressure, rotation speed, rotation pressure and water flow parameters, and the lookout distance. They combine the rotational, hydraulic and percussive mechanisms of the drill, and the confinement of the rock mass by depth. The model has a determination coefficient of 0.74, with the coefficients of the model strongly significant. Residuals are essentially normally distributed. The signs of the exponents indicate that normalized penetration rate, hammer pressure, rotation pressure and the lookout distance inversely influence the excavated distance i.e. high values for them reflect hard, unaltered rock. On the other hand, normalized rotation speed and water flow are directly correlated with the excavated distance, so that high values for them indicate soft, fractured rock.

Acknowledgements

This work has been conducted under the project “TUNEL” (PCD16264900008) funded by the Centre for Industrial Technological Development (CDTI, Government of Spain). The authors would like to thank OSSA Obras Subterráneas SA, for providing the necessary data. The support of MAXAM Civil Explosives is also acknowledged. Special thanks are due to Prof. Håkan Schunnesson of Luleå University of Technology, for his guidance in the MWD normalization analysis. We would also like to thank the anonymous reviewers for their valuable suggestions regarding the analyses and the discussion of the results.

Appendix A. Supplementary material

Supplementary data associated with this article can be found, in the online version, at <https://doi.org/10.1016/j.tust.2018.08.060>.

References

Andersson, P., 1994. The damage zone at tunnel driving, seminar Oct. 1992, SveBeFo report 8. Swedish Rock Engineering Research, Stockholm.

AutoCAD, 2017. Autodesk, Inc.

Barton, N., Lien, R., Lunde, J., 1974. Engineering classification of rock masses for the design of tunnel support. *Rock Mech.* 6 (4), 189–236.

Beattie, N.C.M., 2009. Monitoring-while-drilling for open-pit mining in a hard rock environment: an investigation of pattern recognition techniques applied to rock identification. Doctoral Thesis. Dept. of Mining Engineering, Queen's University, Kingston, Canada.

Costamagna, E., Oggeri, C., Castedo, R., Segarra, P., Navarro, J., 2018. Assessment of contour profile quality in D&B tunneling. *Tunn. Undergr. Space Technol.* 75, 67–80.

Cunningham, C.V.B., Goetzsche, A.F., 1990. The specifications of blast damage limitations in tunnelling contracts. *Tunn. Undergr. Space Technol.* 5, 193–198.

Deere, D.U., Miller, R.P., 1966. Engineering Classification and Index Properties for Intact Rock. Illinois University at Urbana, Department of Civil Engineering.

Fritsch, F.N., Carlson, R.E., 1980. Monotone piecewise cubic interpolation. *SIAM J. Numer. Anal.* 17, 238–246.

Ghosh, R., Schunnesson, H., Kumar, U., 2015. The use of specific energy in rotary drilling: The effect of operational parameters. In: International Symposium on the Application

of Computers and Operations Research in the Mineral Industry: 23/05/2015–27/05/2015.

Ghosh, R., 2017. Assessment of rock mass quality and its effects on charge ability using drill monitoring technique. Doctoral dissertation. Luleå Tekniska Universitet.

Hatherly, P., Leung, R., Scheding, S., Robinson, D., 2015. Drill monitoring results reveal geological conditions in blasthole drilling. *Int. J. Rock Mech. Min. Sci.* 78, 144–154.

Hjelme, J.G., 2010. Drill parameter analysis in the Loren tunnel. M.Sc. thesis in Geosciences. University of Oslo, Department of Geosciences.

Hoek, E., Carranza-Torres, C.T., Corkum, B., 2002. Hoek-Brown failure criterion – 2002 edition. In: Proceedings of the Fifth North American Rock Mechanics Symposium, Toronto, Canada, vol. 1, pp. 267–273.

Hoek, E., 2012. Blast Damage Factor D. Technical note for RocNews, February.

Hu, Y., Lu, W., Chen, M., Yan, P., Yang, J., 2014. Comparison of blast-induced damage between presplit and smooth blasting of high rock slope. *Rock Mech. Rock Eng.* 47 (1), 1307–1320.

Hustrulid, W.A., 1968. Theoretical and experimental study of percussive drilling of rock. Doctoral Thesis. University of Minnesota.

Hustrulid, W., 2010. Some comments regarding development drifting practices with special emphasis on caving applications. *Min. Technol.* 119 (3), 113–131.

Ibarra, J.A., Maerz, N.H., Franklin, J.A., 1996. Overbreak and underbreak in underground openings part 2: causes and implications. *Geotech. Geol. Eng.* 14 (4), 325–340.

Johnson, J.C., 2010. The Hustrulid bar – a dynamic strength test and its application to the cautious blasting of rock. Doctoral Thesis. Department of Mining Engineering, University of Utah.

Kahraman, S., Rostami, J., Naeimipour, A., 2016. Review of ground characterization by using instrumented drills for underground mining and construction. *Rock Mech. Rock Eng.* 49 (2), 585–602.

Kim, Y., Bruland, A., 2009. Effects of drilling and geological parameters on contour quality in a drill and blast tunnel. *Tunn. Undergr. Space Technol.* 24 (5), 584–591.

Kim, Y., Bruland, A., 2015. A study on the establishment of Tunnel Contour Quality Index considering construction cost. *Tunn. Undergr. Space Technol.* 50, 218–225.

Kwon, S., Lee, C.S., Cho, S.J., Jeon, S.W., Cho, W.J., 2009. An investigation of the excavation damaged zone at the KAERI underground research tunnel. *Tunn. Undergr. Space Technol.* 24 (1), 1–13.

Leung, R., Scheding, S., 2015. Automated coal seam detection using a modulated specific energy measure in a monitor-while-drilling context. *Int. J. Rock Mech. Min. Sci.* 75, 196–209.

Liu, H., Yin, K. Karen, 2001. Analysis and interpretation of monitored rotary blasthole drill data. *Int. J. Surf. Min. Reclam. Environ.* 15, 177–203.

Mahdevari, S., Haghghat, H.S., Torabi, S.R., 2013. A dynamically approach based on SVM algorithm for prediction of tunnel convergence during excavation. *Tunn. Undergr. Space Technol.* 38, 59–68.

Mahtab, M.A., Rossler, K., Kalamaras, G.S., Grasso, P., 1997. Assessment of geological overbreak for tunnel design and contractual claims. *Int. J. Rock Mech. Min. Sci.* 34 (3–4), 185–e1.

Mandal, S.K., Singh, M.M., 2009. Evaluating extent and causes of overbreak in tunnels. *Tunn. Undergr. Space Technol.* 24 (1), 22–36.

Matlab, 2017. The MathWorks Inc., Natick, MA.

Naeimipour, A., Bahrampour, S., Rostami, J., Dogruoz, C., 2014. Ground characterization while drilling roofbolters. In: Proceedings of North American Tunneling Conference, 22–25 June, Los Angeles, CA, 11, pp. 51–59.

Navarro, J., Sanchidrián, J.A., Segarra, P., Castedo, R., López, L.M., Cienfuegos, R., 2017. MWD parameters and Drilling Control system. In: Proceedings World Tunnel Congress 2017, 9–15 June 2017, Bergen, Norway, pp. 194–203.

Navarro, J., Sanchidrián, J.A., Segarra, P., Castedo, R., Paredes, C., López, L.M., 2018. On the mutual relations of drill monitoring variables and the drill control system in tunneling operations. *Tunn. Undergr. Space Technol.* 72, 294–304.

NPRA – Norwegian Public Road Administration, 2004. Road Tunnel. Manual 021. ISBN 82-7207-540-7.

Oggeri, C., Ova, G., 2004. Quality on tunneling: ITA-AITES Working Group 16 final report. *Tunn. Undergr. Space Technol.* 19, 239–272.

Olsson, M., 2010. Tunnel blast design for minimizing of the damage zone. A guidance document for SKB and Posiva. Swebrec Report 2010-4, Stockholm, Sweden.

Ouchterlony, F., Olsson, M., Bergqvist, I., 2002. Towards new Swedish recommendations for cautious perimeter blasting. *Fragblast* 6 (2), 235–261.

Peng, S.S., Tang, D., Sasaoka, T., Luo, Y., Finfinger, G., Wilson, G., 2005. A method for quantitative void/fracture detection and estimation of rock strength for underground mine roof. In: Proceedings 24th International Conference on Ground Control in Mining, 2–4 August, Lakeview, WV, pp. 187–195.

Schunnesson, H., 1996. RQD predictions based on drill performance parameters. *Tunn. Undergr. Space Technol.* 11, 345–351.

Schunnesson, H., 1997. Drill process monitoring in percussive drilling for location of structural features, lithological boundaries and rock properties, and for drill productivity evaluation. Doctoral Thesis. Dept. of Environmental Planning and Design, Division of Applied Geology, Luleå University of Technology, Luleå.

Schunnesson, H., 1998. Rock characterization using percussive drilling. *Int. J. Rock Mech. Min. Sci.* 35, 711–725.

Schunnesson, H., Kristofferson, T., 2011. Rock mass characterization using drill and crushability monitoring—A case study. *Int. J. COMADEM.* 14 (2), 44–52.

Schunnesson, H., Elsrud, R., Rai, P., 2011. Drill monitoring for ground characterization in tunnelling operations. In: 20th International Symposium on Mine Planning and Equipment Selection, 12–14 October, Almaty, Kazakhstan.

Schunnesson, H., Pouloupoulos, V., Bastis, K., Pettersen, N., Shetty A., 2012. Application of computerized drill jumbos at the Chenani-Nashri tunnelling site in Jammu-Kashmir, India. In: Proceedings 21st International Symposium on Mine Planning and Equipment Selection, 28–30 November 2012, New Delhi, India, pp. 729–751.

- Schunnesson, H., 2017. Personal communication at Luleå Techniska Universitet, Sweden.
- Scoble, M.J., Peck, J., Hendricks, C., 1989. Correlation between rotary drill performance parameters and borehole geophysical logging. *Min. Sci. Technol.* 8 (3), 301–312.
- Scoble, M.J., Lizotte, Y.C., Paventi, M., Mohanty, B.B., 1997. Measurement of blasting damage. *Mining Engineering*, June 1997, pp. 103–108.
- Singh, P.K., Roy, S.K., Sinha, A., 2003. A new blast damage index for the safety of underground coal mine openings. *Min. Technol.* 112 (2), 97–104.
- Singh, S.P., Xavier, P., 2005. Causes, impact and control of overbreak in underground excavations. *Tunn. Undergr. Space Technol.* 20, 63–71.
- SN – Schweizer Norm, 2004. Conditions générales pour constructions souterraines. SIA – Société suisse des ingénieurs et des architectes, Zurich.
- Tang, X., 2006. Development of real time roof geology detection system using drilling parameters during roof bolting operation. Doctoral Thesis. Department of Mining Engineering, University of West Virginia.
- Teale, R., 1965. The concept of specific energy in rock drilling. *Int. J. Rock Mech. Min. Sci.* 2, 57–73.
- Van Eldert, J., Schunnesson, H., Johansson, D., Saiang, D., 2018. Measurement While Drilling (MWD) technology for blasting damage calculation. In: Proceedings 12th International Symposium on Rock Fragmentation by Blasting, 11–13 June 2018, Luleå, Sweden, pp. 139–148.
- Xu, D.P., Feng, X.T., Chen, D.F., Zhang, C.Q., Fan, Q.X., 2017. Constitutive representation and damage degree index for the layered rock mass excavation response in underground openings. *Tunn. Undergr. Space Technol.* 64, 133–145.
- Yu, T.R., Vongpaisal, S., 1996. New blasting damage criteria for underground blasting. *CIM Bull.* 89 (998), 139–145.